Inorganic Chemistry

Article

pubs.acs.org/IC

Cluster-Based Networks: 1D and 2D Coordination Polymers Based on {$MnFe_2(\mu_3$-O)}-Type Clusters

Galina M. Dulcevscaia,[†] Irina G. Filippova,[†] Manfred Speldrich,[‡] Jan van Leusen,[‡] Victor Ch. Kravtsov,[†] Svetlana G. Baca,*[,§] Paul Kögerler,*[,‡] Shi-Xia Liu,[∥] and Silvio Decurtins[∥]

[†]Institute of Applied Physics, Academy of Sciences of Moldova, Academiei 5, MD-2028 Chisinau, Republic of Moldova

[‡]Institut für Anorganische Chemie, RWTH Aachen University, D-52074 Aachen, Germany

[§]Institute of Chemistry, Academy of Sciences of Moldova, Academiei 3, MD-2028 Chisinau, Republic of Moldova

[∥]Department of Chemistry and Biochemistry, University of Bern, Freiestrasse 3, CH-3012 Bern, Switzerland

Supporting Information

ABSTRACT: A straightforward approach to heterometallic Mn−Fe cluster-based coordination polymers is presented. By employing a mixed-valent μ_3-oxo trinuclear manganese(II/III) pivalate cluster, isolated as $[Mn^{II}Mn^{III}_2O(O_2CCMe_3)_6(hmta)_3]\cdot(solvent)$ (hmta = hexamethylenetetramine; solvent = *n*-propanol (**1**), toluene (**2**)) in the reaction with a μ_3-oxo trinuclear iron(III) pivalate cluster compound, $[Fe_3O(O_2CCMe_3)_6(H_2O)_3]O_2CCMe_3\cdot 2Me_3CCO_2H$, three new heterometallic $\{Mn^{II}Fe^{III}_2\}$ cluster-based coordination polymers were obtained: the one-dimensional polymer chain compounds $\{[MnFe_2O(O_2CCMe_3)_6(hmta)_2]\cdot 0.5MeCN\}_n$ (**3**) and $\{[MnFe_2O(O_2CCMe_3)_6(hmta)_2]\cdot Me_3CCO_2H\cdot(n\text{-hexane})\}_n$ (**4**) and the two-dimensional layer compound $\{[MnFe_2O(O_2CCMe_3)_6(hmta)_{1.5}]\cdot(toluene)\}_n$ (**5**). Single-crystal X-ray diffraction analysis reveals a μ_3-oxo trinuclear pivalate cluster building block as the main constituent in all polymer compounds. Different M:hmta ratios in **1**−**5** are related to the different structural functions of the N-containing ligand. In clusters **1** and **2**, three hmta ligands are monodentate, whereas in chains **3** and **4** two hmta ligands act as bridging ligands and one is a monodentate ligand; in **5**, all hmta molecules act as bidentate bridges. Magnetic studies indicate dominant antiferromagnetic interactions between the metal centers in both homometallic $\{Mn_3\}$-type clusters **1** and **2** and heterometallic $\{MnFe_2\}$-type coordination polymers **3**−**5**. Modeling of the magnetic susceptibility data to a isotropic model Hamiltonian yields least-squares fits for the following parameters: $J_1(Mn^{II}-Mn^{III}) = -6.6$ cm^{-1} and $J_2(Mn^{III}-Mn^{III}) = -5.4$ cm^{-1} for **1**; $J_1 = -5.5$ cm^{-1} and $J_2(Mn^{III}-Mn^{III}) = -3.9$ cm^{-1} for **2**; $J_1(Mn^{II}-Fe^{III}) = -17.1$ cm^{-1} and $J_2(Fe^{III}-Fe^{III}) = -43.7$ cm^{-1} for **3**; $J_1 = -23.8$ cm^{-1} and $J_2 = -53.4$ cm^{-1} for **4**; $J_1 = -13.3$ cm^{-1} and $J_2 = -35.4$ cm^{-1} for **5**. Intercluster coupling plays a significant role in all compounds **1**−**5**.

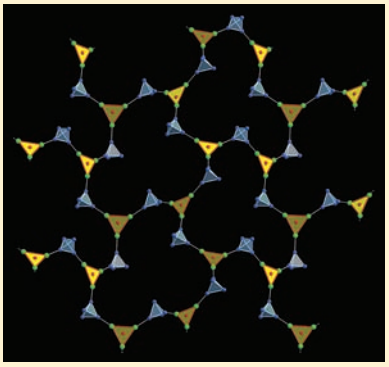

INTRODUCTION

Magnetic coordination polymers have received considerable attention in recent years due to their great potential in the development of "intelligent" multifunctional materials, including magnetic sensors and future spintronic devices, in which the charge transport and tunneling characteristics of such magnetic materials are exploited to realize diode or transistor functionalities.[1,2] One promising approach for the creation of magnetic coordination polymers is based on the assembly of molecular "building blocks" constituted of paramagnetic transition-metal ions and bridging organic linkers. Variation of the size, connectivity, charge, and functionality of complex building blocks and/or ligands then allows us to gain control over the dimensionality of the resulting coordination polymers and, to an increasing degree, impart desired physical properties to the final solid-state materials.[3,4]

Polynuclear carboxylate complexes of Mn(II/III) or Fe(II/III) are especially versatile building blocks, which may be used to construct a diverse range of molecular magnetic arrays and offer numerous advantages: (i) they can exhibit magnetic metastability and hysteresis phenomena that enable magnetic state switching (summarized as single molecule/single-chain magnet features);[2] (ii) the carboxylate ligands can be partially substituted e.g. by redox-active inorganic ligands such as polyoxometalates[5] or organic radical ligands,[6] resulting in increasingly complex magnetic materials with functional properties such as charge-state switching of magnetic ground states and anisotropy; (iii) their terminal ligands frequently are labile, providing an opportunity to assemble the metallic clusters into extended networks through exchange of these terminal ligands by judiciously selected bridging moieties; (iv) they can be deposited and grouped on different surfaces in a controlled manner by functionalizing the peripheral ligands that define their surfaces. Nevertheless, despite the relatively vast body of work focusing on the properties of discrete polynuclear

Received: December 8, 2011
Published: April 23, 2012

   dx.doi.org/10.1021/ic202644t | *Inorg. Chem.* 2012, 51, 5110−5117

Table 1. Crystal Data and Details of Structural Determinations for 1−5

	1	2	3	4	5
empirical formula	$C_{51}H_{98}Mn_3N_{12}O_{14}$	$C_{55}H_{98}Mn_3N_{12}O_{13}$	$C_{43}H_{79.5}Fe_2MnN_{8.5}O_{13}$	$C_{50}H_{95}Fe_2MnN_8O_{15}$	$C_{92}H_{160}Fe_4Mn_2N_{12}O_{26}$
M_r	1268.32	1300.27	1090.29	1214.98	2183.60
T (K)	130(2)	130(2)	150(2)	150(2)	130(2)
cryst syst	hexagonal	monoclinic	orthorhombic	orthorhombic	monoclinic
space group	$P6_3/m$	$P2_1/c$	$Aba2$	$Pbcn$	$P2_1/n$
a (Å)	14.8402(8)	12.3263(9)	23.127(5)	51.2141(12)	17.8948(13)
b (Å)	14.8402(8)	20.8656(15)	24.574(5)	12.2883(3)	23.8818(17)
c (Å)	18.0477(18)	24.9857(17)	19.600(5)	19.6383(4)	25.2878(18)
α (deg)	90	90	90	90	90
β (deg)	90	94.876(1)	90	90	90.634(1)
γ (deg)	120	90	90	90	90
V (Å^3)	3442.2(4)	6403.0(8)	11139(4)	12359.1(5)	10806.3(13)
Z, ρ (Mg m^{-3})	2, 1.224	4, 1.349	8, 1.300	8, 1.306	4, 1.342
μ (mm^{-1})	0.604	0.650	0.800	0.730	0.823
F(000)	1350	2764	4624	5184	4632
cryst size (mm)	0.32 × 0.22 × 0.18	0.28 × 0.25 × 0.17	0.16 × 0.11 × 0.06	0.15 × 0.10 × 0.07	0.27 × 0.20 × 0.14
θ range for data collection (deg)	1.95−27.99	2.03−25.00	1.76−21.97	2.91−24.00	1.42−26.48
index ranges	$-19 \le h \le 19$	$-14 \le h \le 14$	$-24 \le h \le 24$	$-57 \le h \le 45$	$-22 \le h \le 22$
	$-19 \le k \le 19$	$-24 \le k \le 24$	$-25 \le k \le 25$	$-14 \le k \le 8$	$-29 \le k \le 29$
	$-23 \le l \le 23$	$-29 \le l \le 29$	$-20 \le l \le 20$	$-19 \le l \le 22$	$-31 \le l \le 31$
no. of unique/collected rflns (R_{int})	46 549/2863 (0.0674)	50 923/11 271 (0.0501)	32 387/6809 (0.1258)	28 83/9477 (0.0744)	98 441/22 266 (0.0665)
completeness to θ_{max} (%)	100.0	99.9	99.9	97.8	99.6
no. of data/restraints/params	2863/6/127	11 271/0/767	6809/1/628	9477/24/704	22 266/110/1239
final R indices ($I > 2\sigma(I)$)					
R_1	0.0577	0.0375	0.0620	0.0770	0.0491
wR_2	0.1674	0.0962	0.1386	0.1902	0.1289
R indices (all data)					
R_1	0.0702	0.0482	0.0867	0.1273	0.0731
wR_2	0.1783	0.0997	0.15156	0.2047	0.1366
goodness of fit on F^2	1.007	1.007	1.073	0.998	0.961
largest diff peak, hole (e Å^{-3})	0.848, −0.752	1.114, −0.893	0.768, −0.400	1.030, −0.710	1.379, −0.666

coordination clusters of transition metals, including those exhibiting SMM properties, surprisingly little analogous work has been aimed at constructing magnetic cluster-based coordination polymers through the linking of high-nuclearity oxo−metal complexes with nontrivial magnetic properties. There has been a recent effort directed at creating coordination polymers from polynuclear carboxylate clusters by several groups. Christou and Tasiopoulos et al. succeeded in the preparation of one-, two-, and three-dimensional polymers with unprecedented $\{Mn_{17}O_8\}$[7a] or $\{Mn_{19}O_{13}\}$[7b] magnetic building blocks—note that the $\{Mn_{19}\}$-based coordination polymer displays a single-molecule magnet behavior. Linear chain compounds composed of oxo-centered trinuclear $\{Mn_3O\}$[8] or hexanuclear $\{Mn_6O_2\}$[9] carboxylate clusters have also been reported. Among the latter, the $\{Mn_6O_2\}$ pivalate-based compounds with nitronyl nitroxide radical molecules acting as exo-bidentate spacer ligands exhibit SMM properties.[9b] Concerning Fe oxo carboxylate clusters, only a zigzag chain coordination polymer[10] and two-dimensional layers[11,12] that are built up from oxo-centered trinuclear $\{Fe_3O\}$[10,11] or heterometallic $\{Fe_2MO\}$ (M = Co, Ni)[12] carboxylate clusters have been designed.

Recently, we have reported the synthesis and characterization of one-dimensional manganese chain coordination polymers composed of carboxylate cluster blocks with $\{Mn_3O\}$,[13] $\{Mn_4O_2\}$,[13] and $\{Mn_6O_2\}$[14] metallic cores bridged by N-donor ligands and iron chain coordination polymers consisting of the pivalate cluster building units with a $\{Fe_4O_2\}$ metallic core and hmta linkers.[15] In a continuation of this work, we present here convenient synthetic routes to new one- and two-dimensional heterometallic Mn−Fe coordination polymers which are based on the use of mixed-valent μ_3-oxo trinuclear manganese(II/III) pivalate clusters, $[Mn_3O(O_2CCMe_3)_6(hmta)_3]\cdot$(solvent) (hmta = hexamethylenetetramine; solvent = *n*-propanol (**1**), toluene (**2**)) and the homovalent μ_3-oxo trinuclear iron(III) pivalate cluster $[Fe_3O(O_2CCMe_3)_6(H_2O)_3]O_2CCMe_3\cdot 2Me_3CCO_2H$. The resulting network structures include one-dimensional chains in $\{[MnFe_2O(O_2CCMe_3)_6(hmta)_2]\cdot 0.5MeCN\}_n$ (**3**) and $\{[MnFe_2O(O_2CCMe_3)_6(hmta)_2]\cdot Me_3CCO_2H\cdot(n\text{-hexane})\}_n$ (**4**) and two-dimensional layers in $\{[MnFe_2O(O_2CCMe_3)_6(hmta)_{1.5}]\cdot(toluene)\}_n$ (**5**). Herein we focus on the structures and thermal and magnetic properties of these compounds.

EXPERIMENTAL SECTION

Materials and Methods. All reactions were carried out under aerobic conditions using commercial grade solvents. $[Mn(O_2CCMe_3)_2]$ and $[Fe_3O(O_2CCMe_3)_6(H_2O)_3]O_2CCMe_3\cdot 2Me_3CCO_2H$ were synthesized as described elsewhere.[13,16] Commercially available ligands were used without further purification. Infrared spectra were recorded on a Perkin-Elmer Spectrum One spectrometer using KBr pellets in the region 4000−400 cm^{-1}. TGA/DTA measurements were carried out with a Mettler-Toledo TGA/SDTA 851 in dry N_2 (60 mL min^{-1}) at a heating rate of 10 K min^{-1}.

dx.doi.org/10.1021/ic202644t | Inorg. Chem. 2012, 51, 5110−5117

Magnetic susceptibility data were recorded using a Quantum Design MPMS-5XL SQUID magnetometer as a function of field (0.1−5.0 T) and temperature (2.0−290.0 K). Experimental data were corrected for sample holder (PTFE capsules) and diamagnetic contributions calculated from tabulated values (χ_{dia} = −6.370 × 10^{-4} emu mol^{-1} (**1**), −6.501 × 10^{-4} emu mol^{-1} (**2**), −5.410 × 10^{-4} emu mol^{-1} (**3**), −6.057 × 10^{-4} emu mol^{-1} (**4**), −5.461 × 10^{-4} emu mol^{-1} (**5**)). Mn and Fe contents were determined via ICP-OES (Zentralabteilung für Chemische Analysen, Forschungszentrum Jülich).

X-ray Crystallography. Diffraction data sets for **1**−**3** and **5** were collected on a Bruker APEX II diffractometer and for **4** on an Oxford Xcalibur CCD diffractometer, both equipped with graphite-monochromated Mo Kα radiation. A summary of the data collection and the crystallographic parameters of compounds **1**−**5** is given in Table 1. After collection and integration the data were corrected for Lorentz and polarization effects. The structures were solved by direct methods and refined by full-matrix least squares on weighted F^2 values for all reflections using the SHELX suite of programs.[17] All non-hydrogen atoms in clusters **1**−**5** were refined with anisotropic displacement parameters. The disordered atoms of propanol in **1** and acetonitrile molecules in **3** were refined isotropically. Hydrogen atoms were placed in fixed, idealized positions and refined as rigidly bonded to the corresponding atom. In compound **4**, two positions have been specified for hydrogen atoms of three methyl groups. Three different mixed Fe/Mn sites were refined in the same way. In each position the Fe and Mn atoms were constrained to have identical coordinates with site occupation factors of $^2/_3$ for Fe and $^1/_3$ for Mn. The thermal parameters were also constrained to be identical.

Synthesis of Complexes. *$[Mn_3O(O_2CCMe_3)_6(hmta)_3]\cdot nPrOH$ (**1**).* Hexamethylenetetramine (0.16 g, 1.141 mmol) was added to a solution of manganese(II) pivalate (0.3 g, 1.166 mmol) in *n*-propanol (5 mL). The resulting solution was stirred at 60 °C for 1 h and left in an open flask. Dark green crystals suitable for X-ray analysis were filtered off the next day, washed with *n*-propanol and acetonitrile, and dried in air (yield 0.15 g, 31% based on Mn). Anal. Found (calcd) for $C_{51}H_{98}Mn_3N_{12}O_{14}$: C, 48.65 (48.30); H, 7.66 (7.78); N, 13.10 (13.25). IR (KBr pellet, ν/cm^{-1}): 3431 br, w, 2958 m, 2927 sh, 2902 sh, 2874 sh, 1615 vs, 1480 m, 1459 m, 1413 s, 1370 s, 1295 m, 1230 s, 1186 m, 1054 w, 1024 s, 998 vs, 893 w, 867 w, 816 m, 803 m, 777 m, 709 sh, 701 m, 670 m, 660 sh, 599 w.

*Recrystallization of **1** from Hot Toluene To Give $[Mn_3O(O_2CCMe_3)_6(hmta)_3]\cdot(toluene)$ (**2**).* Anal. Found (calcd) for $C_{55}H_{98}Mn_3N_{12}O_{13}$: C, 50.79 (50.80); H, 7.7 (7.6); N, 12.95 (12.93). IR (KBr pellet, ν/cm^{-1}): 2957 m, 2927 sh, 2902 sh, 2873 sh, 1604 vs, 1481 m, 1459 m, 1411 s, 1368 s, 1253 sh, 1229 s, 1054 w, 1024 s, 998 vs, 894 w, 833 w, 806 w, 786 w, 761 w, 710 m, 695 w, 661 m, 599 w.

*$\{[MnFe_2O(O_2CCMe_3)_6(hmta)_2]\cdot 0.5MeCN\}_n$ (**3**).* Compound **1** (0.06 g, 0.0472 mmol), $[Fe_3O(O_2CCMe_3)_6(H_2O)_3]$-$O_2CCMe_3\cdot 2Me_3CCO_2H$ (0.06 g, 0.0521 mmol), and MeCN (5 mL) were placed in a sealed PTFE-lined steel autoclave and heated to 120 °C for 4 h and then slowly cooled to room temperature over 48 h. Crystals of **3** were filtered off, washed with MeCN, and dried in air (yield 0.05 g, 63% based on Fe). Anal. Found (calcd) for $C_{43}H_{79.5}Fe_2MnN_{8.5}O_{13}$: C, 46.69 (47.36); H, 7.41 (7.35); N, 9.67 (10.92); Mn, 5.23 (5.04); Fe, 10.30 (10.24). IR data (KBr pellet, ν/cm^{-1}): 2959 m, 2928 sh, 2873 sh, 1613 sh, 1593 vs, 1551 sh, 1483 vs, 1460 m, 1413 vs, 1371 vs, 1358 vs, 1247 m, 1230 vs, 1051 m, 1023 s, 998 vs, 931 sh, 918 w, 892 w, 828 w, 806 sh, 797 sh, 787 m, 697 s, 680 sh, 663 m, 600 s, 582 sh, 522 m, 429 m.

*$\{[MnFe_2O(O_2CCMe_3)_6(hmta)_2]\cdot Me_3CCO_2H\cdot(n\text{-hexane})\}_n$ (**4**).* A solution of **1** (0.2 g, 0.158 mmol) and $[Fe_3O(O_2CCMe_3)_6(H_2O)_3]$-$O_2CCMe_3\cdot 2Me_3CCO_2H$ (0.2 g, 0.174 mmol) in *n*-hexane (15 mL) was refluxed for 1 h. The warm solution was filtered off and placed in a closed vial at room temperature. Dark green crystals of **4** suitable for X-ray analysis were filtered off after 2−3 days, washed with *n*-hexane, and dried in air (yield 0.13 g, 41% based on Fe). Anal. Found (calcd) for $C_{50}H_{95}Fe_2MnN_8O_{15}$: C, 49.27 (49.24); H, 7.71 (7.88); N, 8.91 (9.22); Mn, 4.37 (4.52); Fe, 8.87 (9.19). IR data (KBr pellet, ν/cm^{-1}): 3433 w, 2958 m, 2928 sh, 2873 sh, 1713 m, 1615 vs, 1595 vs, 1548 sh, 1481 s, 1461 m, 1413 vs, 1371 s, 1293 w, 1246 sh, 1228 vs, 1180 m, 1050 sh, 1022 vs, 997 vs, 933 sh, 919 w, 893 w, 866 w, 826 w, 804 m, 788 w, 776 sh, 758 sh, 696 m, 680 sh, 664 m, 601 m, 583 sh, 525 w, 429 m.

Note that for all syntheses deviations from the reported metal to ligand ratios for the reactants prevented the formation of crystals suitable for single-crystal X-ray diffraction measurements.

*$\{[MnFe_2O(O_2CCMe_3)_6(hmta)_{1.5}]\cdot(toluene)\}_n$ (**5**).* Compound **1** (0.06 g, 0.0472 mmol) was added to a solution of $[Fe_3O(O_2CCMe_3)_6(H_2O)_3]O_2CCMe_3\cdot 2Me_3CCO_2H$ (0.06 g, 0.0521 mmol) in toluene (5 mL). The resulting mixture was refluxed for 6 h and kept in a closed flask. Crystals suitable for X-ray analysis were obtained after 4 days, washed with toluene, and dried in air (yield 0.04 g, 47% based on Fe). Anal. Found (calcd) for $C_{46}H_{80}Fe_2MnN_6O_{13}$: C, 49.88 (50.60); H, 7.47 (7.39); N, 7.76 (7.69); Mn, 5.56 (5.03); Fe, 11.00 (10.23). IR data (KBr pellet, ν/cm^{-1}): 2959 m, 2929 sh, 2873 sh, 1613 vs, 1592 vs, 1542 sh, 1483 s, 1460 m, 1413 vs, 1370 s, 1358 s, 1247 sh, 1225 s, 1051 m, 1022 vs, 996 vs, 928 w, 892 w, 843 sh, 827 w, 797 m, 787 sh, 729 sh, 695 m, 680 sh, 662 sh, 600 m, 582 sh, 520 w, 429 m.

RESULTS AND DISCUSSION

Syntheses and Preliminary Characterization. Trinuclear μ_3-oxo-bridged carboxylate complexes of the type $[M_3O(O_2CR)_6L_3]^{+/0}$ (where M = Mn, Fe; L = H_2O, acid, N-donor ligand) have served as precursors in the synthesis of various multidimensional cluster-based coordination polymers.[7b,8,11,12,15] In this study, the use of μ_3-oxo trinuclear manganese(II/III) and iron(III) pivalate complexes in one-pot reactions in different solvents led to heteronuclear one- or two-dimensional coordination networks. The solvothermal reaction of the μ_3-oxo trinuclear Mn and Fe pivalate complexes with hexamethylenetetramine in MeCN at 120 °C for 4 h in a PTFE-lined stainless autoclave followed by slow cooling to room temperature over 48 h gave the heterometallic chain polymer $\{[MnFe_2O(O_2CCMe_3)_6(hmta)_2]\cdot 0.5MeCN\}_n$ (**3**). In contrast, using the same starting materials, but refluxing in *n*-hexane, afforded the solvated heterometallic chain polymer $\{[MnFe_2O(O_2CCMe_3)_6(hmta)_2]\cdot Me_3CCO_2H\cdot(n\text{-hexane})\}_n$ (**4**). Treatment of trinuclear μ_3-oxo manganese and iron pivalates with a hot toluene solution of hexamethylenetetramine resulted in the precipitation of the 2D heterometallic coordination network $\{[MnFe_2O(O_2CCMe_3)_6(hmta)_{1.5}]\cdot(toluene)\}_n$ (**5**). The yields for **3**−**5** range from ca. 40 to 60%.

The infrared spectra of all complexes **1**−**5** display strong and broad bands in the 1615−1592 and 1413−1411 cm^{-1} regions, arising from asymmetric and symmetric vibrations of the coordinated carboxylate groups of the pivalate ligands, respectively.[18] Solvated pivalic acid in **4** caused the appearance of a band at 1712 cm^{-1} corresponding to vibrations of the uncoordinated carboxylic groups. The C−H asymmetric and symmetric stretching vibrations for the *tert*-butyl group of pivalates are observed in the range 2961−2869 cm^{-1}, along with a strong single band at 1483−1459 cm^{-1} and a doublet at 1371−1358 cm^{-1}, which correspond to asymmetric and symmetric bending vibrations for methyl, respectively. Several well-separated very strong and sharp bands at 1247−1225 and 1024−996 cm^{-1} can be assigned to the C−N stretching modes of the coordinated hmta groups.[19]

Thermogravimetric analyses (25−600 °C) for all compounds were performed under an N_2 flow. TGA data for **1** and **2** show a first mass loss from 90 to 160 °C due to removal of solvent molecules (**1** (*n*PrOH), obsd 4.0%, calcd 4.7%; **2** (toluene),

dx.doi.org/10.1021/ic202644t | Inorg. Chem. 2012, 51, 5110−5117

obsd 10.9%, calcd 7.1%). At higher temperatures organic ligands (six pivalate and three hmta) decompose. For **1**, in the temperature range from 160 to 350 °C a total mass loss of 77.0% (calcd 74.3%) was observed, whereas for **2** from 160 to 470 °C the weight loss amounts to 78.9% (calcd 72.5%). The 1D coordination polymer **3** is stable up to 140 °C, followed by a three-step decomposition of organic constituents up to 470 °C with a total mass loss of 84.9% (calcd 86.5%). For the 1D coordination polymer **4**, in the temperature range of 80−200 °C a 15.4% two-step mass loss corresponds to the release of *n*-hexane and solvate pivalic acid molecules (calcd 15.5%). The decomposition of coordinated pivalate and hmta ligands occurs up to 450 °C (74.5%, calcd 77.6%). For the 2D coordination polymer **5**, the loss of solvate toluene molecules (7.5%, calcd 8.4%) up to 190 °C is followed by decomposition of the metal−organic frameworks in two steps up to 470 °C.

Crystal Structures. The structures of the five μ_3-oxo-centered M_3 compounds $[Mn_3O(O_2CCMe_3)_6(hmta)_3]\cdot n$PrOH (**1**), $[Mn_3O(O_2CCMe_3)_6(hmta)_3]\cdot$(toluene) (**2**), $\{[MnFe_2O(O_2CCMe_3)_6(hmta)_2]\cdot 0.5MeCN\}_n$ (**3**), $\{[MnFe_2O(O_2CCMe_3)_6(hmta)_2]\cdot Me_3CCO_2H\cdot(n\text{-hexane})\}_n$ (**4**), and $\{[MnFe_2O(O_2CCMe_3)_6(hmta)_{1.5}]\cdot$(toluene)$\}_n$ (**5**) have been characterized by single-crystal X-ray diffraction analysis (CCDC 837612−837616). Compounds **1**−**5** share a common similar structural fragment (Figure 1; see Figures S1 and S2 in the Supporting Information for ORTEP plots). Each M site (M = Mn, Fe) in the μ_3-oxo-bridged trinuclear $[M_3O(O_2CCMe_3)_6]$ core fragment adopts a distorted-octahedral geometry and is coordinated to the central μ_3-O atom, four equatorial O centers from four bridging pivalate ligands, and the nitrogen atom of the hmta ligand (trans to μ_3-O). All six pivalates act as bidentate bridging ligands (see Table 2 for metal−ligand bond distances). The different M:hmta ratios in **1**−**5** are related to the different structural functions of the N-containing ligand. In clusters **1** and **2**, all three hmta ligands are monodentate, whereas in chains **3** and **4** two hmta ligands carry out a bridging function and one remains a monodentate ligand; in **5**, all hmta molecules act as bridges.

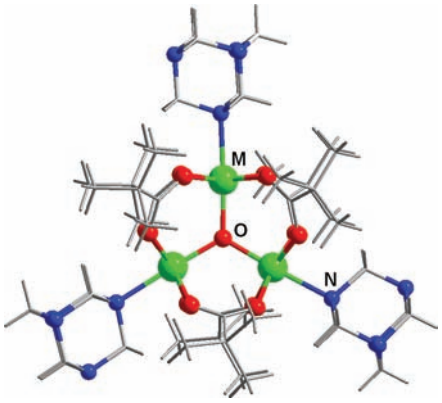

Figure 1. The $[M_3O(O_2CCMe_3)_6(hmta)_3]$ moiety common to compounds **1**−**5**: Fe or Mn, green spheres; N, blue spheres; O, red spheres; C, gray sticks; H, light gray lines.

μ_3-Oxo-Bridged Trinuclear Clusters 1 and 2. The neutral charge of the complexes results in a mixed-valence $Mn^{II}Mn^{III}_2$ composition. In the lattice, the trinuclear clusters in **1** reside around a special position of a 6-fold inversion axis, resulting in a C_{3h}-symmetric planar Mn_3O core and indistinguishable positions of Mn^{II} or Mn^{III} atoms. The Mn−(μ_3-O) distance equals 1.9051(4) Å, Mn−O distances with pivalate ligand are 2.026(2) and 2.030(2) Å, and Mn−N distance is 2.201(3) Å, with a Mn···Mn separation of 3.300(1) Å. The propanol solvent molecule is disorderd around the 6-fold axis. No specific intermolecular interactions have been found between the structural elements (Figure S3, Supporting Information).

The clusters in **2** reside in general position. The Mn−(μ_3-O) [2.136(1) Å] and Mn−N [2.342(2) Å] distances for the Mn2 atom are longer than those for Mn1 [1.832(2) and 2.180(2) Å, respectively] and for Mn3 [1.828(1) and 2.194(2) Å, respectively]. The Mn2−O_{carb} distances are in the narrow range of 2.155(2)−2.169(2) Å, while the Mn1−O_{carb} distances vary from 1.976(2) to 2.176(2) Å and Mn3−O_{carb} from 1.991(2) to 2.154(2) Å. The $Mn_2-O_1-Mn_1$ and $Mn_2-O_1-Mn_3$ angles are equal to 117.82(7) and 116.21(7)°, respectively, while $Mn_1-O_1-Mn_3$ angle is 125.97(8)°. These geometrical parameters show that molecular symmetry of Mn_3O core is close to C_{2v} and that the manganese atoms form an isosceles triangle in contrast to equilateral one in **1**. The data are comparable to known $Mn^{II}Mn^{III}_2O$ trinuclear complexes[20] and assume that the formal oxidation state of Mn2 atom is +II, while the Mn1 and Mn3 oxidation states are +III. In the μ_3-oxo triangle the Mn1···Mn3 separation of 3.260(1) Å is notably shorter than the Mn1···Mn2 [3.401(1) Å] and Mn2···Mn3 [3.369(1) Å] distances. The deviation of the central μ_3-O from the Mn_3 plane centroid is only 0.0024 Å.

One single weak C−H···N interaction can be noticed between the neighboring trinuclear complexes with C···N distance of 3.519(3) Å leading to the formation of 1D hydrogen-bonded chains in **2**. Besides those, the structure of **2** contains the outer-sphere toluene molecules that are connected with the main structural unit through weak C−H···O hydrogen bonds at a distance of 3.482(3) Å (Figure S4).

1D (3 and 4) and 2D (5) Coordination Polymers. The positions of Mn and Fe atoms in M_3O metallic cores of **3**−**5** are undistinguishable from X-ray data. The bond distances in all cases are similar but not regular (Table 2). The M−μ_3-oxygen bond distances in **3**−**5** are in the range of 1.879(5)−1.963(5) Å. The M−O_{carb} bond distances vary from 2.047(6) to 2.084(6) Å in **3**, lie in the range of 2.037(5)−2.092(5) Å in **4**, and 2.031(2)−2.098(2) Å in **5**. Average values of M−O_{carb} bond distances are 2.068, 2.056, 2.063 Å for **3**, **4** and **5**, respectively. The average values of M−N bond distances are 2.359 for **3**, 2.364 for **4**, and 2.382 Å for **5**. Thus, the average bond distances in the core of complexes **3**−**5** are comparable and have intermediate values between the corresponding bond distances for Fe(III) and Mn(II) coordination environments.[21] Valence states in three positions of metal atoms were calculated through a bond valence sum (BVS) analysis,[22] and the BVS values for metal atoms in **3**−**5** are close to each other (2.488−2.787; see Table S6 in the Supporting Information). These parameters assume that Mn and Fe atoms are statistically disordered over three positions in the vertex of the approximately equilateral triangle. Elemental analysis yields the actual Mn:Fe ratio as 1:2 for all coordination polymers **3**−**5**.

The heterotrinuclear clusters in **3** and **4** are connected by two hmta molecules into a similar one-dimensional polymeric chain, as shown in Figure 2. Another similar polymeric chain was found in $\{[Mn^{II}Mn^{III}_2O(O_2CCHMe_2)_6(hmta)_2]\cdot EtOH\}_n$.[13] The third hmta ligand coordinated to the metal atom in the trinuclear cluster is terminal. The distinction in the structural function of hmta ligands occurs in M−N bond

dx.doi.org/10.1021/ic202644t | Inorg. Chem. 2012, 51, 5110−5117

Table 2. Selected Metal−Ligand Bond Distances (Å) for 1−5

					5	
	1	2	3	4		
M1−(μ_3-O)	1.905(4)	1.832(2)	1.879(5)	1.900(4)	1.897(2)	1.935(2)
M2−(μ_3-O)		2.136(1)	1.924(6)	1.963(4)	1.943(2)	1.892(2)
M3−(μ_3-O)		1.828(1)	1.963(5)	1.904(4)	1.929(2)	1.942(2)
M1−O_{carb}	2.026(2)	1.976(2)	2.049(6)	2.037(5)	2.044(2)	2.048(2)
	2.030(2)	1.994(2)	2.060(6)	2.052(5)	2.045(2)	2.071(2)
		2.105(2)	2.068(6)	2.057(5)	2.051(2)	2.077(2)
		2.176(2)	2.079(6)	2.060(5)	2.052(2)	2.093(2)
M2−O_{carb}		2.155(2)	2.047(6)	2.058(5)	2.056(2)	2.029(2)
		2.156(2)	2.060(6)	2.062(5)	2.067(2)	2.031(2)
		2.161(2)	2.064(6)	2.074(5)	2.072(2)	2.050(2)
		2.169(2)	2.074(6)	2.092(5)	2.098(2)	2.072(2)
M3−O_{carb}		1.991(2)	2.071(6)	2.027(5)	2.051(2)	2.062(2)
		1.994(2)	2.073(6)	2.045(5)	2.064(2)	2.073(2)
		2.126(2)	2.083(6)	2.051(5)	2.065(2)	2.080(2)
		2.154(2)	2.084(6)	2.053(5)	2.081(2)	2.088(2)
M1−N	2.201(3)	2.180(2)	2.303(7)	2.332(5)	2.442(3)	2.372(3)
M2−N		2.342(2)	2.403(7)	2.398(6)	2.388(3)	2.381(3)
M3−N		2.194(2)	2.371(8)	2.361(6)	2.355(3)	2.353(3)

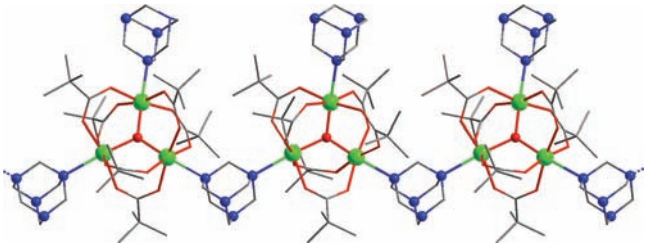

Figure 2. View of the polymeric chain in **3** and **4**: Fe or Mn, green spheres; N, blue spheres; O, red sticks; C, gray sticks. Solvent molecules and hydrogen atoms are omitted for clarity.

distances. There is one short M−N distance for the terminal hmta ligand (2.303(7) Å for **3** and 2.332(5) Å for **4**) and two longer distances (2.371(8) and 2.403(7) Å for **3**; 2.398(6) and 2.361(6) Å for **4**). The M···M distances in **3** are 3.292(2), 3.327(2), and 3.369(2) Å; the out-of-plane deviation of the μ_3-O amounts to 0.029 Å. The corresponding values in complex **4** are 3.298(1), 3.334(1), and 3.355(1) Å and only 0.008 Å for the μ_3-O out-of-plane deviation.

The crystal lattices of **3** and **4** are built up from similar polymeric chains propagating along the *c* axis (Figures S5 and S6, Supporting Information). In accordance with the polar space group *Aba*2 (Table 1) all chains are parallel in the crystal of **3** and antiparallel (alternate in antiparallel directions) in **4**, consistent with the centrosymmetric space group *Pbcn*. If one assume at least partial ordering of the metals in clusters along the chains one may expect the difference in the bulk magnetic properties between **3** and **4**. The intercluster separation within each chain (i.e., the period of the polymer) is equal to approximately *c*/2. The shortest intrachain intercluster M···M distance through the hmta spacer equals 6.591(2) Å in **3** and 6.661(1) Å in **4**. The packing of chains differs in **3** and **4** also because of the template effect of solvent molecules. In **3** the total potential solvent volume equals 1447.2 Å^3 (13%) of the unit cell volume of 11 139.0 Å^3, whereas in **4** the solvent volume equals to 2826.1 Å^3 (22.9%) of the unit cell volume of 12 359.1 Å^3. The shortest interchain M···M distance equals 9.683(3) Å in **3** and 10.249(1) Å in **4**. The cavities in **3** contain solvate acetonitrile molecules, and the channels between chains in **4** are filled by pivalic acid and *n*-hexane molecules. Solvate pivalate molecules form O−H···N = 2.782(1) Å hydrogen bonds with adjacent terminal hmta ligands in the structure of **4**.

The asymmetric unit of **5** contains two similar [$MnFe_2O(O_2CCMe_3)_6(hmta)_{1.5}$] cluster moieties. As mentioned above, the values of bond distances and angles in both crystallographically independent complexes are virtually identical and have intermediate values between those for Fe^{III} and Mn^{II} coordination environments. The M···M separations are 3.325(1), 3.322(1), and 3.344(1) Å in one triangle and 3.310(1), 3.330(1), and 3.350(1) Å in the second complex.

All hmta ligands adopt bridging binding modes and connect neighboring M_3 clusters into a 2D layer structure (Figures 3 and 4). The corrugated layers are parallel to the *ac* plane and are stacked in an ABAB manner. The solvent toluene molecules are disordered into interstitial voids. The intercluster M···M distances through the hmta spacers in **5** are 6.489(1), 6.552(1), and 6.595(1) Å. The shortest M···M distance between layers is 11.151(1) Å. This compares to intercluster M···M separations

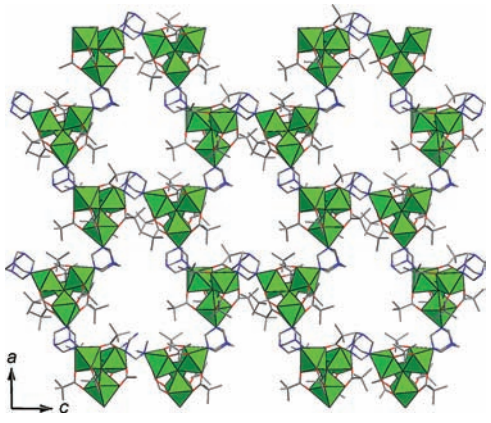

Figure 3. Fragment of the layer of the 2D coordination polymer **5**: metal coordination environments, green polyhedra; N atoms, blue sticks; O atoms, red sticks; C atoms, gray sticks. H atoms and solvate toluene molecules are omitted for clarity.

dx.doi.org/10.1021/ic202644t | *Inorg. Chem.* 2012, 51, 5110−5117

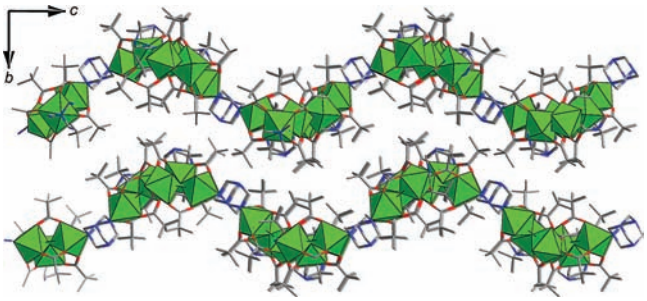

Figure 4. Corrugated layers in **5**. Color codes are as in Figure 3.

of 6.591(2) and 6.611(2) Å in the 1D coordination polymers **3** and **4**, respectively.

Magnetochemical Analysis. The magnetochemical analysis of triangular mixed-valent $\{Mn_3\}$ complexes frequently showcase the limitations of spin-only, isotropic model Hamiltonians, as evident from several published studies of μ_3-O-bridged trinuclear mixed-valent manganese complexes that report isotropic g values between 2.05 and 2.10,[23] although this value should be ≤2.0 for Mn^{II} ($S = {}^5/_2$) and Mn^{III} ($S = 2$) centers in octahedral coordination environments due to ligand-field and spin−orbit coupling effects (Figure S7, Supporting Information). Given that both intra- and intercluster interactions affect the susceptibility data of all presented compounds within the experimental parameter range, we are probing the extent to which the simplest possible model descriptions can accurately reproduce the experimental data, employing our computational framework CONDON 2.0.[24] In the following, isotropic Heisenberg-type exchange coupling assesses all intracluster coupling between spin-only centers, whereas intercluster interactions are taken into account by the molecular field approximation, $\chi_m^{-1} = \chi_m'^{-1} - \lambda_{mf}$, where χ_m' denotes the susceptibility of a discrete $\{M_3\}$ spin cluster, and a negative value of the molecular field parameter λ_{mf} corresponds to net antiferromagnetic intercluster coupling.

The low-field susceptibility data for compounds **1** and **2** (Figure 5) indicate antiferromagnetic magnetic exchange interactions between the spin centers, mediated by μ_3-O and carboxylate bridges as well as the htma groups, and conform to Curie−Weiss expressions only at higher temperatures (χ_m^{-1} vs T only becomes linear above ca. 200 K; see inset in Figure 5). Within the limitations of the employed model, we note that a least-squares fit of the susceptibility data for compounds **1** and **2** containing discrete $\{Mn^{II}Mn^{III}_2\}$ spin clusters to an isotropic Heisenberg-type exchange Hamiltonian for an isosceles spin triangle ($H_{ex} = -2[J_1(S_1 \cdot S_2 + S_2 \cdot S_3) + J_2 S_1 \cdot S_3]$; J_1 parametrizes the two $Mn^{II} \cdots Mn^{III}$ contacts, assumed to be identical, and J_2 the $Mn^{III} \cdots Mn^{III}$ coupling) results in a parameter set with an unrealistic $g_{iso} > 2$. If g_{iso} is constrained to ≤2, the best-fit results are $J_1 = -6.6$ cm^{-1}, $J_2 = -5.4$ cm^{-1}, and $g_{iso} = 2.0$ for **1** and $J_1 = -5.5$ cm^{-1}, $J_2 = -3.9$ cm^{-1}, and $g_{iso} = 2.0$ for **2**; these values reflect the pronounced differences in geometry of the $Mn_3(\mu_3$-O) fragments (see above). The ground states originating from this intramolecular exchange coupling are characterized as $S = {}^1/_2$ for both **1** and **2** (Figure S10, Supporting Information). For both compounds, the quality of the fit increases significantly upon inclusion of intercluster interactions.

Table 3. Results of the Magnetic Analysis for Compounds 1−5

compd	1[a]	2[a]	3	4	5
J_1/cm^{-1}	−6.6	−5.5	−17.1	−23.8	−13.3
J_2/cm^{-1}	−5.4	−3.9	−43.7	−53.4	−35.4
λ_{mf}/mol cm^{-3}	−0.39	−0.17	−0.219	−0.096	−0.051
SQ/%	0.9	1.5	0.8	1.1	1.2

[a]Fits constrained to $g_{iso} \leq 2$.

In compounds **3**−**5** the octahedrally coordinated Mn^{II} and Fe^{III} ($S = {}^5/_2$) ions in the $\{Mn^{II}Fe^{III}_2\}$ clusters are interlinked by htma ligands into polymeric 1D and 2D networks, and intra- and intercluster exchange interactions, as well as weaker coupling between neighboring chains or layers (mediated e.g. by hydrogen bond contacts or involving solvent molecules), again have to be taken into account in modeling the susceptibility data. Here, no linear χ_m^{-1} vs T behavior is observed up to room temperature (Figure 6). For the individual $\{Mn^{II}Fe^{III}_2\}$ cores, the spin Hamiltonian $H_{ex} = -2[J_1(S_1 \cdot S_2 + S_2 \cdot S_3) + J_2 S_1 \cdot S_3]$ describes the intracluster isotropic magnetic exchange interaction. We here assume the exchange interactions involving the two Fe^{III} ions to be equivalent: $J_1 = J_{12} =$

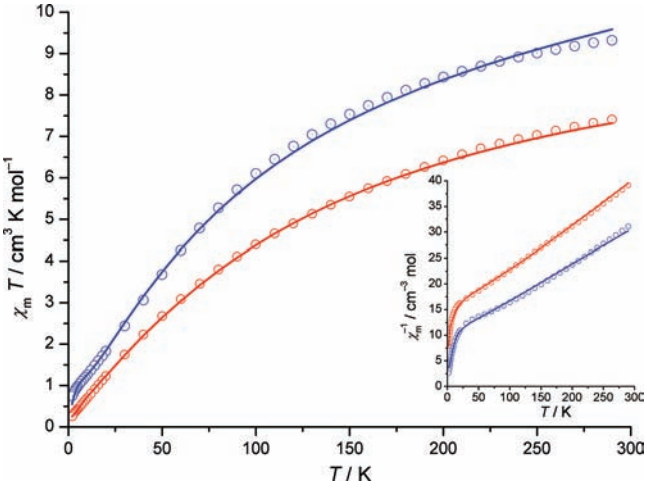

Figure 5. Temperature dependence of $\chi_m T$ (inset: χ_m^{-1}) of **1** (blue) and **2** (red) at 0.1 T: (open circles) experimental data; (solid graphs) least-squares fits to model Hamiltonian (see Table 3 for parameters).

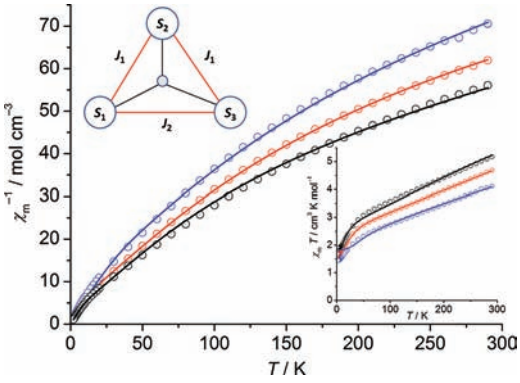

Figure 6. Reciprocal molar susceptibility χ_m^{-1} *vs* T plots of **3** (red), **4** (blue), and **5** (black) at an applied field of 0.1 T: (circles) experimental data, (solid graphs) least-squares fits with parameters given in Table 3. Insets: coupling connectivity for individual $\{MnFe_2\}$ clusters (top; S_1 and S_3, Fe^{III}; S_2, Mn^{II}) and temperature dependence of $\chi_m T$ at 0.1 T (bottom).

dx.doi.org/10.1021/ic202644t | Inorg. Chem. 2012, 51, 5110−5117

J_{23} for the two Mn^{II}–Fe^{III} contacts and $J_2 = J_{13}$ for the Fe^{III}–Fe^{III} contact, i.e. an isosceles spin triangle (Figure 6, inset). The magnetic building block in the 1D chain compounds **3** and **4** can indeed be approximated by an isosceles spin triangle, with one shorter (ca. 3.295 Å, J_2) Fe–Fe and two slightly longer (ca. 3.331 and 3.362 Å, J_1) Mn–Fe contacts. As for compounds **1** and **2**, all intercluster interactions are again modeled using a molecular field model approximation. The two-dimensional heterometallic coordination polymer **5** shows nearly the same magnetic behavior as the 1D chains, but the layer structure does not translate into long-range magnetic ordering. In all three network compounds, the coupling within the $\{Mn^{II}Fe^{III}_2\}$ units results in an effective $S' = {}^3/_2$ ground state, with well-separated first excited states (**3**, 32.3 cm^{-1}, $S = {}^5/_2$; **4**, 47.0 cm^{-1}, $S = {}^1/_2$; **5**, 22.3 cm^{-1}, $S = {}^5/_2$; see Figure S11 in the Supporting Information).

On comparison of the results derived from the isotropic models, both the discrete compounds **1** and **2** and the networked compounds **3**–**5** all exhibit comparable intercluster coupling interactions, which is in part due to the aliphatic backbones of the hmta ligands acting as intercluster superexchange pathways in **3**–**5**. Minor geometric differences of the $M_3(\mu_3\text{-O})(\text{carboxylate})_6$ cluster cores, on the other hand, have the most significant effects on the observed susceptibility data.

CONCLUSION

In summary, the use of μ_3-oxo trinuclear manganese(II/III) and iron(III) pivalate clusters in one-pot reactions has led to a series of new heterometallic $\{Mn^{II}Fe^{III}_2\}$-based coordination polymers in which these μ_3-oxo/pivalate-bridged building blocks are interlinked by hmta ligands into 1D and 2D coordination networks. The solvothermal reaction of these starting materials in MeCN results in the 1D coordination polymer $\{[MnFe_2O(O_2CCMe_3)_6(hmta)_2]\cdot 0.5MeCN\}_n$ (**3**), whereas the same reaction under refluxing in *n*-hexane or toluene produces 1D ($\{[MnFe_2O(O_2CCMe_3)_6(hmta)_2]\cdot Me_3CCO_2H\cdot(n\text{-hexane})\}_n$ (**4**)) and 2D ($\{[MnFe_2O(O_2CCMe_3)_6(hmta)_{1.5}]\cdot(toluene)\}_n$ (**5**)) coordination networks. All of the compounds, manganese clusters (**1** and **2**) and heterometallic Mn–Fe coordination polymers (**3**–**5**), display dominant antiferromagnetic exchange interactions between metal centers, with significant intercluster interactions observed for all compounds. Motivated by these results, the design and synthesis of novel 3D coordination polymers from μ_3-oxo trinuclear carboxylate clusters are currently underway.

ASSOCIATED CONTENT

Supporting Information

CIF files giving X-ray crystallographic data for complexes **1**–**5**, selected bond lengths and angles for **1**–**5** (Tables S1–S5), ORTEP representations of the metal cores in **1**–**5** with atom numbering scheme (Figures S1 and S2), packing diagrams (Figures S3–S6), simulated $\chi_m T$ data for several ligand fields for Mn(III) (Figure S7), field-dependent magnetization (Figures S8 and S9), magnetic energy spectra (Figures S10 and S11), TGA/DTA curves (Figures S12–S16), and BVS values (Table S6). This material is available free of charge via the Internet at http://pubs.acs.org.

AUTHOR INFORMATION

Corresponding Author

*Tel: +49-241-80-93642 (P.K.). Fax: +39-241-80-92642 (P.K.). E-mail: paul.koegerler@ac.rwth-aachen.de (P.K.); sbaca_md@yahoo.com (S.G.B.).

Notes

The authors declare no competing financial interest.

ACKNOWLEDGMENTS

Financial support from the Swiss National Science Foundation (SCOPES IZ73Z0_127925), the German Federal Ministry of Education and Research (project MDA 08/022), the Academy of Sciences of Moldova (project No. 09.820.05.10GF), the Supreme Council for Science and Technological Development of the Republic of Moldova (projects 09.836.05.02A and 11.817.05.03A), and the EU (POLYMAG, IIF contract no. 252984) are acknowledged. We thank Prof. H. Stoeckli-Evans for the collection of crystallographic data sets for compound **1**.

REFERENCES

(1) Batten, S. R.; Neville, S. M.; Turner, D. R. *Coordination Polymers: Design, Analysis and Application*; Royal Society of Chemistry: London, 2009.

(2) Gatteschi, D.; Sessoli, R.; Villain, J. *Molecular Nanomagnets*; Oxford University Press: New York, 2006.

(3) (a) Eddaoudi, M; Moler, D. B.; Li, H.; Chen, B.; Reineke, T. M.; O'Keefee, M.; Yaghi, O. M. *Acc. Chem. Res.* **2001**, *34*, 319. (b) Tranchemontagne, D. J.; Mendoza-Cortes, J. L.; O'Keeffe, M.; Yaghi, O. M. *Chem. Soc. Rev.* **2009**, *38*, 1257. (c) Perry, J. J.; Perman, J. A.; Zaworotko, M. J. *Chem. Soc. Rev.* **2009**, *38*, 1400.

(4) (a) Andruh, M. *Chem. Commun.* **2007**, 2565. (b) Roubeau, O.; Clerac, R. *Eur. J. Inorg. Chem.* **2008**, 4325.

(5) Fang, X.; Kögerler, P. *Chem. Commun.* **2008**, 3396.

(6) (a) Dei, A.; Gatteschi, D.; Sangregorio, C.; Sorace, L. *Acc. Chem. Res.* **2004**, *37*, 827. (b) Miller, J. S. *Inorg. Chem.* **2000**, *39*, 4392. (c) Miller, J. S.; Drillon, M. *Magnetism: Molecules to Materials*; Wiley-VCH: Weinheim, Germany, 2001. (d) McCleverty, J. A.; Ward, M. D. *Acc. Chem. Res.* **1998**, *31*, 842. (e) Kahn, O. *Acc. Chem. Res.* **2000**, *33*, 647. (f) Benelli, C.; Gatteschi, D. *Chem. Rev.* **2002**, *102*, 2369. (g) Mathevert, F.; Luneau, D. *J. Am. Chem. Soc.* **2001**, *123*, 7465.

(7) (a) Moushi, E. E.; Stamatatos, T. C.; Wernsdorfer, W.; Nastopoulos, V.; Christou, G.; Tasiopoulos, A. J. *Inorg. Chem.* **2009**, *48*, 5049. (b) Moushi, E. E.; Stamatatos, T. S.; Wernsdorfer, W.; Nastopoulos, V.; Christou, G.; Tasiopoulos, A. J. *Angew. Chem.* **2006**, *118*, 7886.

(8) (a) Zartilas, S.; Moushi, E. E.; Nastopoulos, V.; Boudalis, A. K.; Tasiopoulos, A. J. *Inorg. Chim. Acta* **2008**, *361*, 4100. (b) Kim, J.; Lim, J. M.; Do, Y. *Eur. J. Inorg. Chem.* **2003**, 2563.

(9) (a) Nakata, K.; Miyasaka, H.; Sugimoto, K.; Ishii, T.; Sugiura, K.; Yamashita, M. *Chem. Lett.* **2002**, 658. (b) Ovcharenko, V.; Fursova, E.; Romanenko, G.; Ikorskii, V. *Inorg. Chem.* **2004**, *43*, 3332. (c) Ma, C. B.; Hu, M. Q.; Chen, H.; Chen, C. N.; Liu, Q. T. *Eur. J. Inorg. Chem.* **2008**, 5274.

(10) Albores, P.; Rentschler, E. *Inorg. Chem.* **2008**, *47*, 7960.

(11) Zheng, Y. Z.; Tong, M. L.; Hue, W.; Zhang, W. X.; Chen, X. M.; Grandjean, F.; Long, G. J. *Angew. Chem., Int. Ed.* **2007**, *46*, 6076.

(12) Polunin, R. A.; Kolotilov, S. V.; Kiskin, M. A.; Cador, O.; Mikhalyova, E. A.; Lytvynenko, A. S.; Golhen, S.; Ouahab, L.; Ovcharenko, V. I.; Eremenko, I. L.; Novotortsev, V. M.; Pavlishchuk, V. V. *Eur. J. Inorg. Chem.* **2010**, 5055.

(13) Baca, S. G.; Malaestean, I. L.; Keene, T. D.; Adams, H.; Ward, M. D.; Hauser, J.; Neels, A.; Decurtins, S. *Inorg. Chem.* **2008**, *47*, 11108.

(14) Malaestean, I. L.; Kravtsov, V. Ch.; Speldrich, M.; Dulcevscaia, G.; Simonov, Y. A.; Lipkowski, J.; Ellern, A.; Baca, S. G.; Kögerler, P. *Inorg. Chem.* **2010**, *49*, 7764.

(15) Baca, S. G.; Filippova, I. G.; Keene, T. D.; Botezat, O.; Malaestean, I. L.; Stoeckli-Evans, H.; Kravtsov, V. Ch.; Chumacov, Iu.; Liu, S.-X.; Decurtins, S. *Eur. J. Inorg. Chem.* **2011**, 356.
(16) Gerbeleu, N. V.; Batsanov, A. S.; Timko, G. A.; Struchkov, I. T.; Indrichan, K. M.; Popovich, G. A. *Dokl. Akad. Nauk SSSR (Russ.)* **1987**, *293*, 364.
(17) Sheldrick, G. M. *Acta Crystallogr.* **2008**, *A64*, 112.
(18) (a) Deacon, G. B.; Philips, R. J. *Coord. Chem. Rev.* **1980**, *33*, 227. (b) Mehrotra, R. C.; Bohra, R. *Metal Carboxylates*; Academic Press: New York, 1983. (c) Nakamoto, K. *Infrared and Raman Spectra of Inorganic and Coordination Compounds*; Wiley: New York, 1986.
(19) Ahuja, I. S.; Singh, R.; Yadava, C. L. *Proc. Indian Acad. Sci. (Chem. Sci.)* **1983**, *92*, 59.
(20) Baca, S. G.; Stoeckli-Evans, H.; Ambrus, Ch.; Malinovskii, S. T.; Malaestean, Iu.; Gerbeleu, N.; Decurtins, S. *Polyhedron* **2006**, *25*, 3617.
(21) Wu, R.; Poyraz, M.; Sowrey, F. E.; Anson, Ch. E.; Wocadlo, S.; Powell, A. K.; Jayasooriya, U. A.; Cannon, R. D.; Nakamoto, T.; Katada, M.; Sano, H. *Inorg. Chem.* **1998**, *37*, 1913.
(22) (a) Brown, I. D.; Altermatt, D. *Acta Crystallogr., Sect. B* **1985**, 244. (b) Brese, N. E.; O'Keeffe, M. *Acta Crystallogr., Sect. B* **1991**, *47*, 192.
(23) Ribas, J.; Albela, B.; Stoeckli-Evans, H.; Christou, G. *Inorg. Chem.* **1997**, *36*, 2352.
(24) Speldrich, M.; Schilder, H.; Lueken, H.; Kögerler, P. *Isr. J. Chem.* **2011**, *51*, 215.